ISSN 8755-6839

SCIENCE OF TSUNAMI HAZARDS

Journal of Tsunami Society International

Volume 40 Number 2 2021

TSUNAMIS FROM STRIKE-SLIP AND NORMAL EARTHQUAKES AND ITS RELATION WITH THE PRODUCT OF DOMINANT PERIOD AND DURATION OF MORE THAN 50 SECONDS OF EARTHQUAKE *P*-WAVE

Madlazim[1], Tjipto Prastowo[1], Muhammad Nurul Fahmi[1], Dyah Permata Sari[1], Ella Melianda[2], Sorja Koesuma[3]

[1]*Universitas Negeri Surabaya, Surabaya 60231, Indonesia*
[2]*Universitas Syiah Kuala, Aceh, Indonesia*
[3]*Universitas Sebelas Maret, Surakarta, Indonesia*
E-mail: madlazim@unesa.ac.id

ABSTRACT

It is widely known that earthquakes with strike-slip or normal-faulting crustal displacements have generated destructive tsunamis around the world. Many researchers have proposed that the main cause of such events was due to factors not associated with tsunami-seismic parameters. However, the present study examines a correlation between tsunamis generated by strike-slip or normal-faulting earthquake events and their associated two tsunami-seismic parameters, namely the dominant period Td and the duration of more than 50 seconds, T50ex of earthquake P-wave, and compares these with tsunami event validity (TEV). Based on this analysis, we confirm a correlation between tsunamis generated by strike-slip or normal-faulting earthquake events with periods $T\text{d} \times T\text{50ex} \geq 10$ s. Thus, we propose that major earthquakes with both strike-slip and normal-fault motions, have the potential to generate more effectively tsunamis when the rupture duration is ≥ 50 seconds and *P*-wave dominant periods have values of $T\text{d} \times T\text{50ex} \geq 10$s.

Keywords: *Tsunami-seismic parameters; P-*wave *Dominant period; P-*wave *duration of more than 50 seconds; Tsunami event validity; strike-slip, normal-faulting earthquakes.*

1. INTRODUCTION

Tsunamis are usually generated by the release of seismic energy on the earth's upper crust, which results in displacements of the sea floor, referred to as earthquake sources. However, besides tectonic mechanisms, tsunamis can be also generated from volcanic sources and submarine landslides (Ward, 2011). Large tsunamis are rarely generated by earthquakes associated with strike-slip or normal-faulting motions. This is due to the fact that strike-slip faults involve primarily horizontal and not vertical crustal movements of the sea floor. Small local tsunamis that may be generated only correlate to insignificantly localized seafloor deformation in size (Gusman *et al*., 2017; Lay *et al*., 2017).

However, historical records indicate that small tsunamis have been generated by strike-slip earthquakes as, for example, that of the 1906 San Francisco, California event (Ma *et al*., 1991; Thatcher *et al*., 1997) and the 1994 Mindoro, Philippines (Imamura *et al*., 1995). Similarly, small tsunamis were generated by more recent events such as the 2016 Kaikoura, New Zealand (Power *et al*., 2017; Ulrich *et al*., 2019a), and the 28 September 2018 Palu, Indonesia earthquakes (Carvajal *et al*., 2019; Ulrich *et al*., 2019b; Madlazim et al., 2020). However, for that Palu earthquake, the major cause of the destructive tsunami remained debatable, since both strike-slip and normal-faulting mechanisms were equally considered responsible. For this event, it has been further proposed that a collateral co-seismic event, such as an undersea landslide may have been a likely source contributing to generation of the tsunami.

Recent work (Muhari *et al*., 2018; Carvajal *et al*., 2019; Heidarzadeh *et al*., 2019) advocated also that a submarine landslide which followed the *M*w 7.5 earthquake on land, disturbed the sea surface and was responsible for the extreme tsunami run-up heights at several places in Palu Bay. Contrary to this, Ulrich *et al*. (2019b) proposed a model of co-seismic earthquake parameters to find an oblique component in addition to a slip faulting type for the event, causing a significant vertical seafloor displacement of 1.5 m across a segment underneath Palu-Koro fault. This finding was supported by aerial evidence from satellite imagery, confirming surface deformation associated with the event and its corresponding ruptured segment (Madlazim and Supriyono, 2014; Socquet *et al*., 2019). Furthermore, other studies (Goda *et al*., 2019; Gusman *et al*., 2019) argued for a combined source mechanism of vertical seafloor displacement and a complex undersea landslide following mainshocks. Using the combined source model, they successfully resolved the surveyed run-up heights and the corresponding tsunami inundation, as documented by the subsequent field surveys.

Using both duration more than 50 seconds, τ_{50ex} and the dominant period, τ_d acquired from teleseismic data, Lomax and Michelini (2009b; 2011) showed that the parameters could be potential tsunami discriminants. Madlazim *et al*. (2013), using local Indonesian events, confirmed the importance of the parameters on assessing tsunami hazard. Regarding the dependence of tsunami excitation on seafloor displacement, Lomax and Michelini (2013) further used these parameters for effective early warning within five minutes. Using a total of 300 Indonesian events, independently of source mechanisms, Madlazim *et al*. (2019) made this limitation shortened by a minute with no false warning in the reported case studies .

Although a better understanding of reliable tsunami discriminants for rapid analysis and assessment of tsunami potential has developed in time, the roles played by tsunami importance Λ first defined in Lomax and Michelini (2009b) and the product of $\tau_d \times \tau_{50ex}$ discussed in Lomax and Michelini (2011), along with the inclusion of earthquake characterization, remain questionable for accurate tsunami early warning. In particular, a correlation between tsunamigenic earthquakes of strike-slip or normal-faulting origin and the corresponding tsunamis induced in terms of probability to occur, in percentage, for a set of seismic data given for both source mechanisms, independent of epicenter location, is of paramount importance. Knowledge about this issue may help parameterize tsunami excitation aftershocks, hence improve the reliability of tsunami early warning. Therefore, this study aims to analyze past tsunamis around the world generated by strike-slip and normal earthquakes' and its relation with the product of dominant period and duration more than 50 seconds of earthquake *P*-wave.

2. METHODS

Estimates of τ_d were performed using a direct procedure with no inversion at the initiation, making the calculation process relatively shortened. The first step of τ_d estimates were to determine time domain τ_c according to Lomax and Michelini (2011) as follows,

$$\tau_c = 2\pi T2 T1 v2 dt dT2 T1 \acute{v}2 dt \quad (1)$$

where $T1$ = 0 (the onset time of *P*-waves) and $T2$ = 55 s acquired from teleseismic data (Lomax and Michelini, 2009). Detailed steps of τ_d estimates are as follows: (1) preparing raw earthquake data records from the vertical velocity component of broadband seismogram in a miniseed format, (2) applying 4-poles and a corner frequency of 0.05 Hz Butterworth bandpass filter to obtain the high-frequency, vertical component of velocity records for each seismic station; (3) picking *P*-wave arrival times automatically at the high-frequency, vertical-velocity seismogram; (4) integrating the seismogram and comparing it with vertical acceleration component of broadband seismogram times 2π of arrival times of *P*-waves automatically picked up from the vertical-velocity records on the high-frequency seismogram; and (5) the final results were values of τ_d.

$$T_{50Ex} = A_{50}/A_{RMS} \quad (2)$$

Where A_{50} is average amplitude for 50 to 60 seconds, and A_{RMS} is average amplitude for 0 to 25 seconds.

The followings are detailed steps of determining the $\bar{\tau}50ex$ exceeding 50 s using a direct procedure: (1) preparing raw data from the vertical component of broadband seismogram in a miniseed format, (2) applying 4-poles and the 5-20 Hz Butterworth band pass filter to obtain the high-frequency, vertical component of seismic velocity for each seismic station used; (3) picking arrival times of *P*-waves automatically at the high-frequency, vertical-velocity seismogram; (4) calculating the RMS-amplitude and $\bar{\tau}50$ values; and (5) estimating $\bar{\tau}50ex$ using the ratio of $\bar{\tau}50$ to the RMS-amplitude values.

The estimated values for τ_d, and $\bar{\tau}50ex$ are compared with Tsunami Event Validity (TEV). Validity of the actual tsunami occurrence is indicated by a numerical rating of the reports of that event: -1 is erroneous entry indication of erroneous entry, 0 is indication of event that only caused a seiche or disturbance in an inland river, 1 is indication of very doubtful tsunami, 2 is indication of questionable tsunami, 3 is indication of probable tsunami, and 4 is indication of definite tsunami (National Geophysical Data Center / World Data Service: NCEI/WDS Global Historical Tsunami Database. NOAA National Centers for Environmental Information. doi:10.7289/V5PN93H7). The detailed algorithms above for calculations of τ_d, and $\bar{\tau}50ex$ were implemented into Jokotingkir, a programming package that Madlazim *et al*. (2019) used both local and regional events to accurately calculate the three seismic parameters for improved tsunami early warning within four minutes after the main shocks, which can be accessed at http://prediksi-tsunami.unesa.ac.id/www/

The product of $\tau_d \times \bar{\tau}50ex$ was chosen here as it was proved to bring more information about potentially induced tsunamis by earthquakes than other discriminants, the moment magnitude M_w (both are included in Table 1 but are then excluded in calculations for cross-correlation techniques presented in the current work). As pointed out by Necmioglu and Özel (2014), rupture duration determination has a relatively large uncertainty affecting tsunami initiation and hence being improper for tsunami hazard assessment. A similar situation to occur was found for earthquake magnitude, scaled with any measure,

as the magnitude was proved to be inaccurate for tsunami analysis and assessment (Madlazim and Prastowo, 2016). The data were acquired from a network of seismic stations on the basis of local observations available from the Indonesian Agency for Geophysics, Climatology, and Meteorology (BMKG) at http://202.90.198.100/webdc3/, regional and teleseismic data provided by the German Research Centre for Geosciences, known as GEOFON GFZ accessed at http://eida.gfz-potsdam.de/webdc3/ and the Incorporated Research Institutions for Seismology-Data Management Center (IRIS-DMC) available at http://www.iris.edu/wilber3/find_event. We used direct procedures of calculation for relatively quick assessment of tsunami generation potential using earthquake source parameters, including the dominant period τ_d, the rupture duration τ_{dur} and the apparent rupture duration τ_{50ex} longer than 50 s from velocity records on the high-frequency *P*-waves seismogram.Top of Form Bottom of Form

3. RESULTS AND DISCUSSIONS

We considered how estimates of τ_d and τ_{50ex} were carried out. These events are associated with the movement of a left-lateral strike-slip and normal fault system in the world. Estimation of τ_d and T_{50Ex} was performed using the direct procedure previously presented. Note that all the observed values for τ_{dvand} τ_{50ex} estimates are higher than their respective thresholds at $\tau_d \geq 10$ s and $\tau_{50ex} \geq 1$, respectively, for tsunami generation potential proposed by Lomax and Michelini (2011). The same finding as field observations, and both eyewitnesses and video-footages collected (Carvajal *et al*., 2019; Goda *et al*., 2019).

Our tasks now are examining earthquake datasets from all the events considered in this study and classifying them using the two sensitive correlation parameters for tsunami excitation, namely $\tau_d \times \tau_{50ex} \geq 10$ s. We are here intent to use global tsunamigenic earthquake datasets to test whether such requirement holds for strike-slip or normal-faulting mechanisms around the globe. Each event was monitored by nearby stations locate at, on average, 478.87 km and far stations situated in, on average, 1922.66 km away from the epicenter. Each event was recorded at >25 stations at epicentral distances of $10^o - 60^o$. The point to make is that the discriminant $\tau_d \times \tau_{50ex}$ is used to examine the independence of the events on a further catastrophe, *i.e*., the events being not always followed by landslides. A total of 35 events consisting of 19 strike-slip and 16 normal-faulting mechanisms, centered either on the mainland or at sea, were analyzed, and the results were then provided in detail in Table 1. For each event, $\tau_d \times \tau_{50ex}$ was first determined after rapid calculations of τ_d and τ_{50ex}. The next step was to correlate the product of $\tau_d \times \tau_{50ex}$ to TEV ≥ 3 of the same event whether they both fulfill $\tau_d \times \tau_{50ex} \geq 10$ s. When one of these does not meet the requirement, we can then say they are not correlated.

Table 1. Tsunami parameter estimation results from strike-slip and normal-faulting earthquakes

No	Origin Time (UTC)	Lat	Long	D (km)	M w	Td (s)	T50 ex	Td × T50ex (s)	TEV	Event	Type	Status
1	19941114 19:15:30	13.5° N	121.1° E	31.5	7.0	5.7	0.8	4.7	4	nT	So	FW
2	19990817 00:01:38	40.7° N	29.9° E	17.0	7.6	16.8	1.8	30.4	4	T	Sc	TW
3	20021010 10:50:22	1.7° S	134.3° E	24.8	7.5	8.0	1.6	9.3	1	nT	So	TW
4	20090528 08:24:48	16.8° N	86.2° W	29.0	7.3	10.2	1.4	14.2	4	T	So	TW
5	20100112 21:53:10	18.4° N	72.6° W	15	7	3.7	1.5	5.6	4	T	Sc	TW
6	20100226 20:31	25.9° N	128.4° E	25.0	7.0	6.6	0.4	2.9	3	nT	So	FW
7	20101225 13:16:38	19.8° S	167.9° E	15.7	7.3	11.5	1.5	16.9	4	T	No	TW
8	20110109 10:03:43	19.3° S	168.4° E	20.7	6.5	5.6	1.7	10.5	4	T	No	TW
9	20110510 08:55:12	20.3° S	168.3° E	33.4	6.8	9.2	1.0	11.5	4	T	No	TW
10.	20110624 03:09:38	51.9° N	171.8° W	49.8	7.3	5.1	1.9	12.8	4	T	No	TW
11	20110706 19:03:2	29.3° S	176.2° W	25.4	7.6	10.2	2.1	21.2	4	T	No	TW
12	20110710 00:57:10	38.1° N	143.3° E	24.7	7.0	5.4	1.5	11.0	4	T	No	TW
13	20120202 13:34:41	17.8° S	167.2° E	27.3	7.0	7.1	1.3	10.1	4	T	No	TW
14	20120309 07:09:53	19.2° S	169.8° E	33.7	6.6	6.7	0.9	12.5	4	T	No	TW
15	20120411 08:38:37	2.2° N	93.0° E	26.3	8.6	9.4	1.9	18.3	4	T	So	TW
16	20120411 10:43:10	0.8° N	92.4° E	21.6	8.2	7.8	2.0	15.8	4	T	So	TW
17	20130105 08:58:19	55.2 ° N	134.8 ° W	3.1	7.5	14.1	1.6	22.5	4	T	So	TW
18.	20130208 15:26:38	10.9° S	166.2° E	22.4	7.0	4.9	1.6	8.1	4	nT	So	FW
19.	20130419 03:05:52	46.1° N	150.9° E	109	7.2	2.8	2.8	7.8	2	nT	No	TW

No	Origin Time (UTC)	Lat	Long	D (km)	M w	Td (s)	$T50$ ex	Td × $T50$ex (s)	TEV	Event	Type	Status
20	20141014 03:51:37	12.5° N	88.1° W	63.9	7.3	4.8	1.4	13.7	4	T	No	TW
21	20150710 04:12:42	9.3° S	158.3° E	20.0	6.7	7.2	1.1	7.8	4	T	So	TW
22	20150718 02:27:32	10.4° S	165.1° E	11.8	6.9	9.3	1.7	15.9	4	T	No	TW
23	20160302 12:49:48	4.95° S	94.3° E	24.0	7.8	8.4	2.0	17.1	4	T	So	TW
24	20160812 01:26:36	22.4° S	173.1° E	16.44	7.2	9.4	1.1	10.7	4	T	So	TW
25	20161121 20:59:49	37.3° N	141.4° E	11.35	6.9	8.8	2.3	19.9	4	T	No	TW
26	20161113 11:02:59	42.7° S	173.1° E	22.0	7.8	11.0	1.9	20.8	4	T	Sc	TW
27	20170103 21:52:30	19.3° S	176.1° E	126.9	6.9	9.5	0.7	13.9	4	T	No	TW
28	20170717 23:34:13	54.4° N	168.8° E	10.99	7.7	7.6	1.6	12.3	4	T	So	TW
29	20170908 04:49:20	15.0° N	93.9° W	56.67	8.1	7.2	2.4	17.2	4	T	No	TW
30	20180110 02:51:31	17.4° N	83.5° W	10	7.5	11.1	1.8	20.2	4	T	So	TW
31	20180123 09:31:42	56.0° N	149.0° W	25	7.9	2.7	2.6	6.9	4	nT	So	FW
32	20180928 10:02:43	0.2° S	119.8° E	10.0	7.5	8.4	1.9	15.9	4	T	Sc	TW
33	20181211 02:26:32	58.5° S	26.5° W	164.6	7.1	10.4	1.7	18.1	0	T	No	FW
34	20181205 04:18:08	21.9° S	169.4° E	10	7.5	8.6	1.5	12.9	4	T	No	TW
35	20200128 19:10:24	19.4° N	78.8° W	14.8	7.7	8.8	1.7	14.7	4	T	So	TW

Notes: Sc (Continental Strike-Slip Fault), So (Oceanic Strike-Slip Fault), Nc (Continental Normal Fault), No (Oceanic Normal Fault), FW (False Warning = unrelated), TW (True Warning = related), T (Tsunami), nT (non Tsunami).

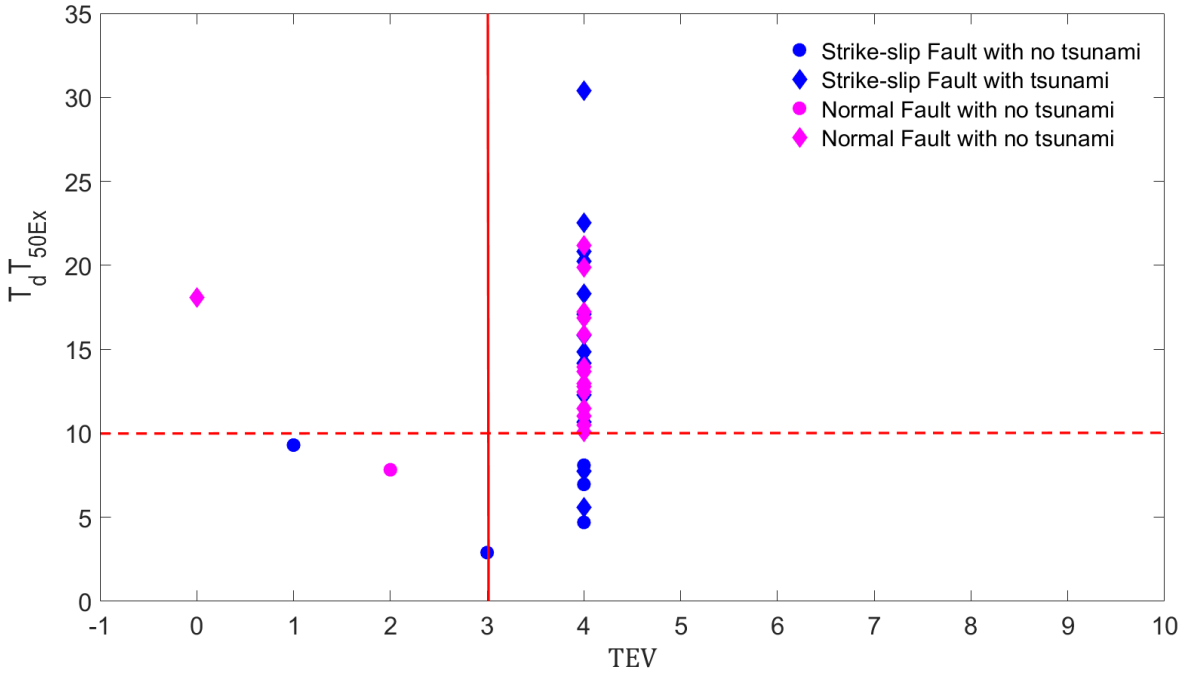

Fig 1. The relationship between $T_d \times T_{50ex}$ and TEV. The vertical red line shows the threshold value of TEV and the horizontal red line shows threshold value of $T_d \times T_{50ex}$. diamond shows a tsunami event and a circle shows a non-tsunami event.

In Fig. 1 for strike-slip cases, there exist 15 events where $T_d \times T_{50ex} \geq 10$ s and TEV ≥ 3 are satisfied and related, leaving the requirement unrelated for other 4 events in this type of energy release mechanism. While, for normal-faulting, almost all, which are 15 of 16, show a positive correlation. From a total of 35 events considered, about 86% of all the events, or 30 occurrences, take both the requirement simultaneously. These include 15 strike-slip and 14 normal-faulting mechanisms. It follows that both mechanisms can be potential sources of tsunami generation as long as the requirement meets and in particular, rupture movement is directed towards the seafloor. This finding also provides insight into a possibility that the tsunamigenic earthquake, independent of source mechanism, is then possibly centered on land or at sea. A well-known example of this is a tsunami wave that hit Kaikoura region in New Zealand on 13 November 2016 (Power *et al*., 2017; Ulrich *et al*., 2019a) several minutes after the main shock occurred in the region. Another example from a recent local event is the one when a propagating tsunami wave penetrating into Palu Bay on the 28 September 2018 Palu, Indonesia (Carvajal *et al*., 2019; Ulrich *et al*., 2019b).

Cases where $T_d \times T_{50ex}$ and TEV < 3 are uncorrelated, meaning that only one of these relations $T_d \times T_{50ex} \geq 10$ s or TEV ≥ 3 is satisfied, are accounted for a total of 9 earthquake events consisting of 8 events due to strike-slips and one event related to normal-faulting. For a special case where $T_d \times T_{50ex} \geq 10$ s does not hold but TEV ≥ 3 is satisfied; we here argue for some possible factors that are not related to seismic source parameters, for example, an underwater landslide, inducing tsunami generation. In oppose to this, for a situation where $T_d \times T_{50ex} \geq 10$ s holds but TEV ≥ 3 is no longer the case; the possible reason is that a tsunami wave is generated at a location in the open ocean far away from beaches and propagates towards the shorelines with much reduction in its wave energy. Hence, when the wave approaches near the shorelines, its height is measured by local tide-gauges insignificantly, causing no much destruction on areas near the shores.

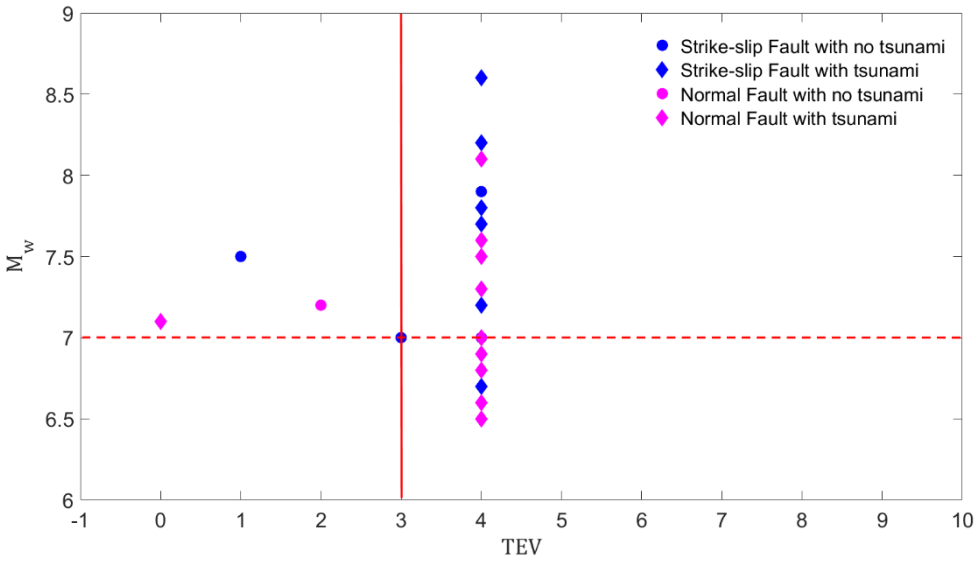

Fig 2. The relationship between *M*w and TEV. The vertical red line shows the threshold value of TEV and the horizontal red line shows threshold value of *Mw*. Triangle shows a tsunami event and a circle shows a non-tsunami event.

If viewed from the correlation between the parameters Mw and TEV as in Figure 2, for the case of the strike-slip earthquake from 19 events there are 10 events that fulfill these two parameters and the other 9 only fulfill one of them. Meanwhile, in normal earthquake cases, there are also 10 correlated events and 6 not. If in the total of the entire event, there are 71% or as many as 24 earthquakes that meet the requirements for the Mw and TEV parameters. If the two parameters are correlated, it can be said that the tsunami that occurred was caused by a large magnitude earthquake which had an amplitude of more than 0.5 m and could have occurred near the coastline, while for cases where only the Mw parameter was met it means that the tsunami wave was likely generated at a location in the open ocean far from the coast and spreading to the shoreline with much reduction in wave energy so that the amplitude is less than 0.5 m, and for cases where only the TEV is satisfied there may be other sources affecting TEV ≥ 3, one example is an underwater landslide.

Table 2. The calculation results of tsunami potential use different discriminants

Discriminant	Available (min after OT)	Treshold Value	True Warning			False warning		
			TEV$\geq$3	TEV < 3	%**	TEV$\geq$3	TEV < 3	%**
M_w	5-10	7.0	24	1	71%	7	3	29%
$\tau d \times \tau 50ex$	5	10.0	28	2	86%	4	1	14%

** Percent of true warning and false warning

Table 2 shows that the correlation of parameters $\tau d \times \tau 50ex$ and TEV correctly identifies 86% of the tsunami events caused by strike-slip earthquakes and normal earthquakes, more than the correlation of M_w and TEV which is only 71%. This is because the Mw parameter cannot identify earthquakes that have a magitude moment of less than 7.0 which have a long rupture duration (Lomax and Michelini, 2009A). Therefore, the parameter $\tau d \times \tau 50ex$ is better used than the parameter Mw for tsunami early warning.

4. CONCLUSIONS

We have examined two tsunami-seismic parameters, the dominant period T_d and the likely apparent rupture-duration T_{50ex} that exceeds 50 s in the form of a calculated value $T_d \times T_{50ex}$ and a value characterizing tsunami importance I_t. We have then used these values as good measures considering $T_d \times T_{50ex} \geq 10$ s generation using a total of 35 earthquakes initiated by 19 strike-slip and 16 normal-faulting movements of varying source locations worldwide. Twenty sixes of the events, approximately 86%, of these 35 events with various focal mechanisms are positive related to generate tsunamis or no tsunamis, where strike-slip earthquakes contribute 43% to tsunami excitation, and normal-earthquakes take a greater portion of 43%. The results suggest that, in terms of relative contribution, the slightly large portion given by the normal faults and the strike-slips earthquakes are ability to relate of tsunamis or no tsunamis.

ACKNOWLEDGEMENTS

We firmly acknowledge GEOFON GFZ and Incorporated Research Institutions for Seismology (IRIS) for which seismic data were available from their respective sites at http://eida.gfz-potsdam.de/webdc3/ and http://www.iris.edu/wilber3/find. This work is funded by DRPM, The Ministry of Education and Culture, The Republic of Indonesia under grant number 217/SP2H/LT/DRPM/2021.

.

REFERENCES

Carvajal, M., Araya-Cortejo, C., Sépulveda, I., Melnick, D. & Haase, J. S., 2019. Nearly instantaneous tsunamis following the M_w 7.5 2018 Palu earthquake, *Geophys. Res. Lett.,* **46**, 1-33, doi:10.1029/2019GL082578

Geist, E. L. & Bilek, S. L., 2001. Effect of depth-dependent shear modulus on tsunami generation along subduction zones, *Geophys. Res. Lett.*, **28**(7), 1315-1318.

Goda, K., Mori, N., Yasuda, T., Prasetyo, A., Muhammad, A. & Tsujio, D., 2019. Cascading geological hazards and risks of the 2018 Sulawesi Indonesia earthquake and sensitivity analysis of tsunami inudation simulations, *Front. Earth Sci.*, **7**(261), doi:10.3389/feart.2019.00261.

Goldstein, P. & Snoke, A., 2005. SAC availability for the IRIS community. United States. *Incorporated Research Institutions for Seismology Newsletter* **7**(1).

Gusman, A. R., Satake, K., & Harada, T., 2017. Rupture process of the 2016 Wharton Basin strike‐slip faulting earthquake estimated from joint inversion of teleseismic and tsunami waveforms. *Geophys. Res. Lett.*, **44**, 4082-4089, doi:10.1002/2017GL073611.

Gusman, A. R., Supendi, P., Nugraha, A. D, Power, W., Latief, H., Sunendar, H., Widiyantoro, S., Daryono, Wiyono, S. H., Hakim, A., Muhari, A., Wang, X., Burbidge, D., Palgunadi, K., Hamling, I. & Daryono, M. R., 2019. Source model for the tsunami inside Palu Bay following the 2018 Palu earthquake, Indonesia. *Geophys. Res. Lett.*, **46**(15), 8721-8730, doi:10.1029/2019GL082717.

Heidarzadeh, M., Muhari, A. & Wijanarko, A. B., 2019. Insights on the source of the 28 September 2018 Sulawesi tsunami, Indonesia based on spectral analyses and numerical simulations. *Pure Appl. Geophys.*, **176**, 25-43, doi:10.1007/s00024-018-2065-9.

Imamura, F., Synolakis, C. E., Gica, E., Titov, V., Listanto, E. & Lee, H. J., 1995. Field survey of the 1994 Mindoro Island, Philippines tsunami. *Pure Appl. Geophys.*, **144**(3-4), 875-890, doi:10.1007/BF00874399.

Lay, T., Ye, L., Bai, Y., Cheung, K. F., & Kanamori, H., Freymueller, J., Steblov. G. M. & Kogan, M. G., 2017. Rupture along 400 km of the Bering fracture zone in the Komandorsky islands earthquake (M_W 7.8) of 17 July 2017. *Geophys*. *Res*. *Lett*., **44**(12), 12161-12169, doi:10.1002/2017GL076148.

Lomax, A. & Michelini, A., 2009a. Mwpd: a duration-amplitude procedure for rapid determination of earthquake magnitude and tsunamigenic potential from *P*-waveforms, *Geophys. J. Int*., **176**, 200-214, doi:10.1111/j.1365-246X.2008.03974.x.

Lomax, A. & Michelini, A., 2009b. Tsunami early warning using earthquake rupture duration, *Geophys*. *Res*. *Lett*., **36**, L09306, doi:10.1029/2009GL037223.

Lomax, A. & Michelini, A., 2011. Tsunami early warning using earthquake rupture duration and *P*-wave dominant period: the importance of length and depth of faulting. *Geophys*. *J. Int*., **185**(1), 283-291.

Lomax, A. & Michelini, A., 2013. Tsunami early warning within five minutes. *Pure Appl. Geophys.,* **170**, 1385-1395, doi:10.1007/s00024-012-0512-6.

Ma, K-F., Satake, K. & Kanamori, H., 1991. The origin of the tsunami excited by the 1906 San Francisco earthquake, *Bull*. *Seismol*. *Soc*. *Am*., **81**(4), 1396-1397.

Madlazim, 2013. Assessment of tsunami generation potential through rapid analysis of seismic parameters-case study: comparison of the Sumatra earthquakes of 6 April and 25 October 2010, *Sci*. *Tsu*. *Hazards* **32**(1), 29-38.

Madlazim & Prastowo, T., 2016. Evaluation of earthquake parameters used in the Indonesian Tsunami Early Warning System, *Earthq*. *Sci*. **29**(1), doi:10.1007/s11589-016-0143-6.

Madlazim, Rohadi, S., Koesoema, S. & Meilianda, E., 2019. Development of tsunami early warning application four minutes after an earthquake. *Sci*. *Tsu*. *Hazards* **38**(3), 132-141.

Madlazim and Supriyono, 2014. Improving Experiment design skills: Using the Joko program as a learning tool of tsunami topic. *Sci. Tsu. Hazards*. **33**(2), 133-143

Madlazim, Prastowo, T., Fahmi, M.N. 2020. Estimation of Rupture Directivity, CMT And Earthquake Tsunami Parameters And Their Correlation with The Main Source of The First Tsunami Wave, September 28, 2018. Science of Tsunami Hazards . Nov2020, Vol. 39 Issue 4, p228-242. 15p.

Muhari, A., Imamura, F., Arikawa, T., Hakim, A., & Afriyanto, B., 2018. Solving the puzzle of the September 2018 Palu, Indonesia, tsunami mystery: clues from the tsunami waveform and the initial field survey data, *J. Disaster Res*., **13**, sc20181108, doi:10. 20965/jdr.2018.sc20181108.

Necmioglu, Ö. & Özel, N. M., 2014. An earthquake source sensitivity analysis for tsunami propagation in the eastern Mediterranean, *Oceanog*., **27**(2), 76-85, doi:10.5670/oceanog.2014.42.

Power, W., Clark, K., King, D. N., Borrero, J., Howarth, J. & Lane, E. M., 2017. Tsunami runup and tide-gauge observations from the 14 november 2016 M7.8 Kaikoura earthquake, New Zealand. *Pure Appl*. *Geophys*., **174**(7), 2457-2473.

Socquet, A., Hollingsworth, J., Pathier, E., & Bouchon, M., 2019. Evidence of supershear during the 2018 magnitude 7.5 Palu earthquake from space geodesy. *Nat*. *Geosci*., **12**, 192-199, doi:10.1038/s41561-018-0296-0.

Thatcher, W., Marshall, G. & Lisowski, M., 1997. Resolution of fault slip along the 470-km-long rupture of the great 1906 San Francisco earthquake and its implications, *J. Geophy*s. *Res*., **102**, B3, 5353-5367.

Ulrich, T., Gabriel, A. A., Ampuero, J. P. & Xu, W., 2019a. Dynamic viability of the 2016 Mw 7.8 Kaikoura earthquake cascade on weak crustal faults. *Nat*. *Commun*., **10**(1), 1213. doi:10.1038/s41467-019-09125-w.

Ulrich, T., Vater, S., Madden, E. H., Behrens, J., van Dinther, Y., van Zelst, I., Fielding, E. J., Liang, C. & Gabriel, A. A., 2019b. Coupled, physics-based modeling reveals earthquake displacements are critical to the 2018 Palu, Sulawesi Tsunami, *Pure Appl*. *Geophys*., **176**(32), 4069-4109, doi:10.1007/s00024-019-02290-5

Ward, S. N. 2011. *Encyclopedia of Solid Earth Geophysics: Tsunami.* Edited by Harsh K. Gupta. National Geophysical Research Institute (NGRI). Council 51 of Scientific and Industrial Research (CSIR). Springer Netherlands: Dordrecht, Netherlands, 1-1539. e-ISBN: 978-90-481-8702-7.